Atmos. Chem. Phys. Discuss., 11, 5019–5042, 2011
www.atmos-chem-phys-discuss.net/11/5019/2011/
doi:10.5194/acpd-11-5019-2011

Atmospheric Chemistry and Physics Discussions

Measurements of gaseous H_2SO_4 by AP-ID-CIMS during CAREBeijing 2008 Campaign

J. Zheng[1], M. Hu[2], R. Zhang[1,2], D. Yue[2], Z. Wang[2], S. Guo[2], X. Li[2,5], B. Bohn[5], M. Shao[2], L. He[3], X. Huang[3], A. Wiedensohler[4], and T. Zhu[2]

[1]Department of Atmospheric Sciences, Texas A&M University, College Station, TX 77843-3150, USA
[2]State Key Joint Laboratory of Environmental Simulation and Pollution Control, College of Environmental Sciences and Engineering, Peking University, Beijing 100871, China
[3]Key Laboratory for Urban Habitat Environmental Science and Technology, Shenzhen Graduate School of Peking University, Shenzhen 518055, China
[4]Leibniz Institute for Tropospheric Research, Permoserstrasse 15, Leipzig 04318, Germany
[5]Institute für Energie- und Klimaforschung Troposphäre (IEK-8), Forschungszentrum Jülich, 52425 Jülich, Germany

Received: 19 January 2011 – Accepted: 27 January 2011 – Published: 10 February 2011

Correspondence to: M. Hu (minhu@pku.edu.cn)

Published by Copernicus Publications on behalf of the European Geosciences Union.

Abstract

As part of the 2008 Campaign of Air Quality Research in Beijing and Surrounding Regions (CAREBeijing 2008), measurements of gaseous sulfuric acid (H_2SO_4) have been conducted at an urban site in Beijing, China from 7 July to 25 September 2008 using atmospheric pressure ion drift – chemical ionization mass spectrometry (AP-ID-CIMS). This represents the first gaseous H_2SO_4 measurements in China. Diurnal profile of sulfuric acid is strongly dependent on the actinic flux, reaching a daily maximum around noontime and with an hourly average concentration of 5×10^6 molecule cm^{-3}. Simulation of sulfuric acid on the basis of the measured sulfur dioxide concentration, photolysis rates of ozone and nitrogen dioxide, and aerosol surface areas captures the trend of the measured H_2SO_4 diurnal variation within the uncertainties, indicating that photochemical production and condensation onto preexisting particle surface dominate the observed diurnal H_2SO_4 profile. The frequency of the peak H_2SO_4 concentration exceeding 5×10^6 molecule cm^{-3} increases by 16% during the period of the summer Olympic Games (8–23 August 2008), because of the implementation of air quality control regulations. Using a multivariate statistical method, the critical nucleus during nucleation events is inferred, containing two H_2SO_4 molecules ($R^2 = 0.85$). When neither nucleation nor precipitation occurs, the condensation rate of H_2SO_4 correlates with the daytime sulfate mass concentration of the Aitken mode, but not with that of the accumulation mode aerosols.

1 Introduction

Gaseous sulfuric acid (GSA) is of critical atmospheric interest for its important role in various atmospheric processes, such as new particle formation (Seinfeld and Pandis, 1998; Finlayson-Pitts and Pitts, 1999) and modification of optical properties and hygroscopicity of preexisting aerosols (Khalizov et al., 2009a, b). GSA is predominantly formed through the gas-phase reaction between hydroxyl radical (OH) and sulfur dioxide (SO_2) in the presence of oxygen (O_2) and water (H_2O),

ACPD
11, 5019–5042, 2011

$$SO_2 + OH + M \rightarrow HSO_3 + M \quad \text{(R1)}$$

$$HSO_3 + O_2 \rightarrow SO_3 + HO_2 \quad \text{(R2)}$$

$$SO_3 + H_2O + M \rightarrow H_2SO_4 + M \quad \text{(R3)}$$

GSA forms strong inter-molecular hydrogen bonds with H_2O, and H_2SO_4 has a low saturation vapor pressure at atmospherically relevant relative humidity (Zhang et al., 1993; Zhao et al., 2009). The fate of GSA in the atmosphere depends on the available surface area of preexisting aerosols. H_2SO_4 also forms molecular complexes with inorganic and organic species (Zhang et al., 2004). The size of these complexes is usually less than a few nanometers, below the detection limit of conventional instrumentation for nanoparticles. New particle formation includes nucleation to form the critical nucleus and subsequent growth of the critical nucleus to a detectable size of nanoparticles (L. Wang et al., 2010; Zhang, 2010). Although the detailed mechanisms of atmospheric aerosol nucleation and growth is still a subject of active research (Kulmala et al., 2004; Arnold, 2006; Nadykto and Yu, 2007; Young et al., 2008; Sipila et al., 2010; Zhang, 2010), H_2SO_4 is commonly considered as one of the dominant components of newly formed nanoparticles.

Atmospheric aerosols have important implications on the solar and terrestrial radiation budget (IPCC, 2007; Zhang et al., 2008), and multi-phase chemical processes (Molina et al., 1997). Freshly emitted soot contains mainly elementary carbon (EC) and to a lesser extent organic matter (OM). EC absorbs solar and terrestrial radiation and is also referred to as black carbon (BC). Fresh soot is largely hydrophobic and does not serve as cloud condensation nuclei (CCN) until a high supersaturation is reached (Zhang et al., 2008). However, after exposure to GSA, soot particles become hydrophilic, because of irreversibly uptake of GSA (Zhang and Zhang, 2005). Consequently, aged soot is more prone to wet deposition and has a smaller atmospheric residence time. Internally mixed soot particles with H_2SO_4 (or neutralized by ammonia to form ammonium sulfate) enhance light absorption and scattering, especially at

ACPD
11, 5019–5042, 2011

higher mass fraction of sulfate (Cheng et al., 2008; Khalizov et al., 2009a). GSA significantly influences the soot-ageing process by modifying the morphology, optical properties, and hygroscopicity of soot particles (Zhang et al., 2008). Measurements of GSA provide a valuable input for evaluation of the soot aging process under atmospheric conditions. Furthermore, sulfuric acid can efficiently catalyze aqueous reactions of organic compounds, formed from photo-oxidation of volatile organic compounds (Suh et al., 2001; Zhang et al., 2002b), contributing to the formation of secondary organic aerosols (Zhao et al., 2005, 2006).

Because of rapid economic development and urbanization, Beijing has become one of the most populated cities in China. Increasing demand for energy in both industrial and domestic sectors leads to large fossil fuel consumption, with annual emissions of 2.39×10^5 tons of nitrogen oxides ($NO_x = NO + NO_2$), 2.4×10^5 tons of volatile organic compounds (VOCs), 1.9×10^5 tons of SO_2, and 5.8×10^4 tons of soot (Chan and Yao, 2008). Consequently, Beijing is frequently experiencing severe air pollution events, which are characterized by high concentrations of ozone (O_3) and particulate matter (PM) and severe deterioration in visibility. Rapid soot aging has been reported in the Beijing area, when the single scattering albedo of the aerosols increases to values above 0.9 within several hours due to secondary aerosol formation and condensation growth (Cheng et al., 2009).

Because of concerns on air quality during the 2008 Olympic Games period, the Beijing Municipal Environmental Protection Bureau (EPB) adopted a series of air quality control measures (Wang et al., 2009). On 20 July, a rule for odd/even numbers of the registration plate of automobiles was applied, aiming a reduction of 50% of the traffic volume from the private car sector. During the Olympic Games period, extra 20% of state owned vehicles were off the road, but extra diesel buses were added to public transportation fleet to accommodate the increasing demand for public traffic among different stadiums. After the Paralympics ended on 17 September, most of the regulations were lifted and on-road traffic increased. The Campaign of Air Quality Research in Beijing and Surrounding Regions (CAREBeijing 2008) was one of a series

ACPD
11, 5019–5042, 2011

of comprehensive field studies (e.g., CAREBeijing 2006 and 2007) targeting the understanding of the chemical and physical processes responsible for the air pollution episodes. During the CAREBeijing 2008 campaign, a suite of state-of-the-art instruments were deployed to measure trace gases, meteorological parameters, and aerosol number size distribution and chemical compositions (PM_1).

This paper reports measurements of GSA during the CAREBeijing 2008 field study. In a separate publication, the role of GSA in new particle formation and growth has been investigated by Yue et al. (2010). Data validation of the GSA measurements is performed using a normalized sequential difference analysis (NSD). Meteorological effects on GSA are also discussed. The GSA diurnal features are presented and the influences from the administrative regulations on GSA measurements are discussed. Moreover, the fate of GSA in the Beijing urban environment is evaluated, focusing on its photochemical production and condensation sink. By applying a multivariate statistical method, the number of H_2SO_4 molecules in the critical nuclei is estimated during nucleation events. The contribution of H_2SO_4 to particulate sulfate is assessed.

2 Experimental

2.1 GSA measurements

The observation site was on the rooftop of a six-story building on the campus of the Peking University (39°59′21″ N and 116°18′26″ E), located in the NW part of the urban Beijing area. GSA was measured with atmospheric pressure ion-drift chemical ionization mass spectrometry (AP-ID-CIMS). The detailed instrument description has been provided elsewhere (Fortner et al., 2004; Zheng et al., 2010). Briefly, the AP-ID-CIMS consisted of an inlet (10 cm ID and 60 cm long), an Am-241 ion source, an atmospheric pressure ion-drift tube, and a quadrupole mass spectrometer (QMS). The AP-ID-CIMS was housed inside an air-conditioned observatory. To minimize wall loss, the inlet was machined into a scooped-shape and the sampling rate was kept at about

ACPD
11, 5019–5042, 2011

1200 standard liters per minute (slpm). About 55 slpm of the total air sample was introduced into the drift tube, where ambient H_2SO_4 underwent proton-transfer reactions with nitrate anion ($NO_3^-{\cdot}HNO_3$) (*m/e* 125), generated from HNO_3 vapor by α particle radiation, to form $HSO_4^-{\cdot}HNO_3$ (*m/e* 160). All reagent and product ions were sequentially monitored by the QMS in selective ion monitor (SIM) mode for about 12 s. Instrument calibrations were conducted twice a week with a custom-made water photolysis GSA primary source adjustable in the concentration range of 10^7 to 10^8 molecules cm^{-3}. For a 5 min average time, the detection limit for GSA was about 10^5 molecules cm^{-3}. From in-situ calibrations, the sensitivity of AP-ID-CIMS (counts per second (Hz) per unit H_2SO_4 molecule cm^{-3}) varied within 36% of the mean value and was reported as the uncertainty in the present work.

2.2 Aerosol and trace gas measurements

Aerosol number size distribution (3 nm to 10 µm) was measured by a twin differential mobility particle sizer (TDMPS) and an aerodynamic particle sizer (APS) (TSI Inc., model 3321). The TDMPS consists of two Hauke-type differential mobility analyzers and two condensation particle counters (TSI Inc., model 3010 and 2025) and are used to measure the particle size distributions from 3 to 900 nm (Stokes diameter). The APS is used to measure aerosols with aerodynamic diameter between 500 nm and 10 µm. A detailed description and operation conditions of the TDMPS and APS are provided by Yue et al. (2010). The concentration of particle surface area is integrated from the particle number distribution, by assuming a spherical geometry for the particle.

An Aerodyne High-Resolution Time-of-Flight Aerosol Mass Spectrometer (HR-ToF-AMS) was deployed to characterize particle chemical compositions. The detailed instrumental description of HR-ToF-AMS has been given by DeCarlo et al. (2006). The operation procedure of the HR-ToF-AMS during the 2008 CAREBeijing campaign has been described by Huang et al. (2010) in a companion paper of this special issue. Briefly, the HR-ToF-AMS was operated sequentially in a cycle of 5 modes every 10 min, including a 2 min V-mode to obtain the mass concentrations of the non-refractory

ACPD
11, 5019–5042, 2011

species, a 2 min W-mode to obtain high resolution mass spectral data, a 4 min separate PToF (particle time-of-flight) mode to determine size distributions of species under the V-mode, and a 2 min Soft-EI mode using a lower EI voltage (~13 eV).

The photolysis frequencies of O_3 (J_{O^1D}) and NO_2 (J_{NO_2}) were measured by specifically designed filter radiometers provided by Forschungszentrum Jülich, Germany (FZJ). The instruments were calibrated at FZJ with a reference spectroradiometer before and after the campaign. The accuracy of the photolysis frequency measurements was estimated to be 10% at solar zenith angles smaller than 80° (Bohn et al., 2008).

Measurements of meteorology parameters including wind direction, wind speed, temperature, pressure, relative humidity, precipitation, UVA and UVB were conducted with a LASTEM auto meteorology station (LSI-LASTEM, M7115). SO_2 was measured with a commercial fluorescence sulfur dioxide analyzer (ECTECH, E9850). Both instruments were maintained and calibrated routinely.

3 Results and discussion

3.1 Instrument performance and meteorological effect

Accurate measurements of GSA represent a great challenge because of its low concentration. A normalized sequential difference (NSD) analysis of the GSA data is performed to evaluate the performance of the AP-ID-CIMS instrument. NSD at time t is calculated from (Arnold et al., 2007)

$$\mathrm{NSD}_t = \frac{C_t - C_{t-1}}{\sqrt[2]{C_t \times C_{t-1}}} \quad (1)$$

where C_t and C_{t-1} correspond to two consecutive GSA data points at time t and $t-1$, respectively. NSD represents the consistency of the instrument performance. Since all the factors affecting the observation results are random in nature, NSD_t is expected to exhibit a normal distribution with a mean of zero if there is not a systematic bias

ACPD
11, 5019–5042, 2011

associated with the instrument. Figure 1a shows the frequency histogram of the NSD plotted in bins of 0.023 width. The histogram appears to be nearly a Gaussian distribution with a slight positive skewness. A *p*-value of 0.24 (larger than 0.05) is obtained from a standard t-test between the NSD and a randomly generated normal distribution with the same standard deviation as the calculated NSD but a mean value of zero, indicating that the positive skewness is statistically insignificant. Therefore, the GSA data shows no systematic instrument bias in either direction. Similarly, by plotting NSD with GSA concentration (Fig. 1b), it is demonstrated that within the observed GSA concentration range, the NSD is also normally distributed, i.e., the AP-ID-CIMS does not show a systematic bias within the range of observed GSA level.

GSA is highly sticky to almost all kind of surfaces. In order to minimize the inlet losses, a short inlet and a high sampling flow rate are used for the GSA measurement. The inlet is made of a 10 cm ID aluminum tube, which significantly reduces diffusion. Turbulence induced wind gust may impact GSA measurements. Figure 2 presents (a) a polar plot of the NSD with wind direction (North = 0°) and (b) a scatter plot of NDS with wind direction. Overall, NSD scatters in all wind direction with a slight bias under NW wind, but NSD is symmetrically distributed at any wind speed. This result is explained by the orientation of the inlet, i.e., when wind blows from perpendicular to the inlet or at a higher speed, more wall loss is expected as the air flow changes direction for both cases, but this bias is statistically insignificant.

3.2 H_2SO_4 measurements

The measurement period spans from 7 July to 25 September, covering the entire period of the XXIX Olympic Games and the Paralympics. Because GSA is photochemically produced and readily lost to aerosol surfaces, its concentration is expected to follow solar radiation intensity and is anti-correlated with the aerosol loading. Figure 3 shows the time series of GSA concentration measured during the 2008 CAREBeijing field campaign. The gaps within the series are due to interruption of power supply or instrument calibration. Diurnally, GSA typically remains a minimum value from late night

ACPD
11, 5019–5042, 2011

to early morning and reaches a daily peak at noontime. The maximum peak value of GSA is measured on 10 September, with a concentration of 1.9×10^7 molecules cm^{-3}.

The reaction between SO_2 and OH (Reactions R1 to R3) represents the primary pathway to form GSA (Finlayson-Pitts and Pitts, 1999), whereas GSA is readily removed by condensing onto aerosol surfaces. Simultaneous measurements of GSA and aerosol surface area present a unique opportunity to evaluate the competition between production and removal of GSA. The steady-state GSA concentration is calculated from

$$P_{GSA} = L_{GSA} \tag{2}$$

where $P_{GSA} = k_{OH+SO_2}[OH][SO_2]$ and $L_{GSA} = \frac{\gamma \cdot S \cdot \bar{v}}{4}[H_2SO_4]$ (Freiberg and Schwartz, 1981), P_{GSA} and L_{GSA} denote GSA production and loss, respectively, k_{OH+SO_2} is the rate constant of Reaction (R1) (JPL, 2006), $\bar{v}$ is the mean velocity of GSA molecules, S is the aerosol surface concentration (μm^2 cm^{-3}), and γ is the uptake coefficient of GSA on aerosol surface. A value of 0.73 (Jefferson et al., 1997) is adopted for γ. Because OH is not measured in this work, the OH concentration is estimated according to Ehhalt and Rohrer (2000),

$$[OH] = a(J_{O^1D})^{\alpha}(J_{NO_2})^{\beta}\frac{bNO_2 + 1}{cNO_2^2 + dNO_2 + 1} \tag{3}$$

where J_{O^1D} and J_{NO_2} are observed photolysis rates of O_3 and NO_2, respectively. The values of the constants are taken from Ehhalt and Rohrer (2000), i.e., $a = 4.1 \times 10^9$, $b = 140$, $c = 0.41$, $d = 1.7$, $\alpha = 0.83$, and $\beta = 0.19$. It has been suggested that Eq. (3) is valid under high NO_x conditions, which is typically the case in the megacity Beijing with large NO_x emissions (Liu and Shao, 2007). Because only dry deposition is considered in Eq. (2), GSA measurements when precipitation occurs are excluded in this investigation. Figure 4a shows hourly average diurnal plots of the measured aerosol surface area, SO_2, and calculated OH concentration. Figure 4b displays both the hourly average GSA measurements with one σ error bar and calculated GSA from

ACPD
11, 5019–5042, 2011

Eq. (2). Daytime GSA reaches a daily maximum around noontime with a value of $\sim 5 \times 10^6$ molecules cm^{-3}. The calculated GSA captures the measured trend in general, indicating that photochemistry dominates the GSA production. However, since photochemistry is the only source considered, nighttime GSA cannot be accounted for. Given that the lifetime of GSA relative to aerosol uptake is less than a minute, the nighttime concentration of GSA ($\sim 1 \times 10^6$ molecules cm^{-3}) clearly indicates that other non-photochemical mechanism is operative to produce OH radicals, such as the ozonolysis of alkenes (Zhang et al., 2002a; Fan and Zhang, 2004). The planetary boundary layer height typically reaches the minimum in the early morning and grows rapidly within a few hours after sunrise. As a result, surface air pollutants are vented upward and air masses of the regional sources are mixed down, explaining the variations in the particle surface area concentration and SO_2 concentration. Both OH and GSA are photochemically driven and their concentrations show clear variations with the solar diurnal cycle.

Another interesting feature in Fig. 3 is that the measured GSA peak value exhibits a periodic variation of about one week. Such a variation is related to the aerosol loading, which is regulated by the large-scale weather pattern in this area. A change in the weather pattern, such as the wind direction (from northwest) or precipitation, leads to a cleaner air condition, allowing GSA to reach a higher concentration.

In order to improve air quality during the Olympic Games, control measures have been implemented to reduce primary air pollutant emissions, especially, from industries, on-road vehicles and construction sites. Considerable reductions in both gas-phase and aerosol-phase pollutants have been observed by both mobile laboratory (Wang et al., 2009) and surface stations (T. Wang et al., 2010). Moreover, more precipitation and cleaner conditions associated with the northerly wind were experienced during the period. Consequently, more "Blue-Sky" days were observed during the Olympic Games in the Beijing region (Zhang et al., 2010). Since GSA production is enhanced by stronger actinic flux and uptake by preexisting aerosol surfaces represents the dominant sink for GSA, an increasing trend in the daily GSA concentration is

ACPD
11, 5019–5042, 2011

evident in Fig. 3, especially during the Olympics and Paralympics period, when more stringent traffic control measures were adopted. For example, the frequency of the peak H_2SO_4 concentration exceeding 5×10^6 molecule cm^{-3} increases by 16% during 8–23 August, compared to the time period prior to 8 August. This trend is consistent with that of the frequency of new particle formation events (Yue et al., 2010).

3.3 H_2SO_4 in new particle formation

During the CAREBeijing 2008 campaign, fourteen nucleation events were observed, which has been discussed previously in a companion paper in this special issue (Yue et al., 2010). In this work, a multivariate statistical method (MSM) (McGraw and Zhang, 2008) is employed to analyze the molecular components of the critical nuclei during eleven nucleation events. Table 1 summarizes new particle formation rate (FR) and GSA measurements.

To perform the MSM analysis, a multicomponent extension form of the kinetic nucleation theorem (Ford, 1997) is deduced by treating the critical clusters as the transition state during the nucleation process, i.e., the nucleation rate is determined from the sum of flux of each condensable gas that contributes to the growth of clusters over the critical size. Details of the MSM analysis for aerosol nucleation are described by (McGraw and Zhang, 2008). Applying the data listed in Table 1, we find that the most likely number of H_2SO_4 molecules in the critical clusters is 2. This is consistent with the result by Anderson et al. (2008), who suggest that at least two sulfuric acid molecules are required to form a stable critical cluster. It should be pointed out that other species, including organics, can also be presence in the critical nucleus (Zhang et al., 2004, 2009; Metzger et al., 2010), but cannot be concluded from our present analysis.

3.4 Contribution of GSA to particulate sulfate

To evaluate the likely contribution of GSA to particulate sulfate, we compare the calculated condensation rates to the measured sulfate mass concentrations by the

ACPD
11, 5019–5042, 2011

HR-ToF-AMS. Figure 5 shows the diurnal profiles of the calculated GSA condensation rates for the Aitken and accumulation modes, which are evaluated using Eq. (2). The aerosol surface area of each mode is integrated from TDMPS number size distribution measurement. Also shown in Fig. 5 for comparison are diurnal profiles of the corresponding aerosol sulfate mass concentrations for the Aitken and accumulation modes measured by the HR-ToF-AMS. Limited by the sampling efficiency of the HR-ToF-AMS, we define Aitken and accumulation modes as 40 to 100 nm and 100 to 400 nm in Stokes diameters, respectively. Both modes of aerosol sulfate show signature of predominant secondary formation, i.e., the lowest concentration in the early morning and the highest concentration in either the afternoon or early evening. The calculated GSA condensation rate in both modes is strongly influenced by the GSA concentration (Fig. 4b). For the Aitken mode aerosols, the calculated GSA condensation rate exhibits a close correlation with the measured concentration of sulfate mass from the HR-ToF-AMS. This may imply that condensation of GSA (followed by neutralization with ammonia) dominates particle growth in the mode. In contrast, for the case of accumulation mode aerosols, the increase in the concentration of sulfate mass from the HR-ToF-AMS is noticeably delayed than that of the calculated GSA condensation rate, suggesting that GSA condensation hardly contributes to the growth in this mode. Instead, the growth in accumulation mode aerosols is more likely to be explained by inter-modal coagulation.

It has been suggested by Guo et al. (2010) that fine mode sulfate in the Beijing area can arise from secondary sources, since biomass burning and automobile exhausts also contribute to fine particles. Also, according to He et al. (2010), sulfate production through the aqueous phase reaction between hydrogen peroxides (H_2O_2) and SO_2

$$SO_2 + H_2O \leftrightarrow HSO_3^- + H^+ \quad \text{(R4)}$$

$$HSO_3^- + H_2O_2 \rightarrow HSO_4^- + H_2O \quad \text{(R5)}$$

in aqueous aerosols is not significant during the CAREBeijing 2008 campaign. Other possible sulfate production mechanisms include heterogeneous reactions on the

ACPD
11, 5019–5042, 2011

aerosol surface or in-cloud processing (Seinfeld and Pandis, 1998). Future work, especially a detailed aerosol dynamic model along other aerosol and gaseous measurements, is required to quantitatively assess the contributions of GSA condensation, inter-modal coagulation, and other sulfate production mechanisms to the measured sulfate mass concentrations in the Aitken and accumulation modes.

4 Conclusions

As part of the CAREBeijing 2008 field study, GSA measurement by AP-ID-CIMS was conducted at an urban site in Beijing City from 7 July 2008 to 25 September 2008. This represents the first GSA measurements in China. Data quality is examined using a normalized sequential difference procedure. GSA data set shows no statistically significant systematic errors. Correlations between GSA and meteorology parameters are also analyzed. Only a minor bias is identified when the wind direction is perpendicular to the sample inlet, likely due to turbulence-induced wall losses. Diurnally, GSA shows strong dependence on actinic flux and reaches daily maximum around noon, ranging from a few 10^6 to 1.9×10^7 molecules cm^{-3}. Nighttime GSA ($\sim 1 \times 10^6$ molecules cm^{-3}) is also observed, indicating that non-photochemical OH sources are operative in Beijing, such as the ozonolysis of alkenes. Traffic control and other administrative measures pertaining to the Olympic Games period appear to be effectively improving air quality in Beijing with significant reduction in aerosol loading, which is consistent with the observation that GSA daily maximum is noticeably increased from the beginning to the later part of the campaign. On the basis of the assumption that GSA concentration is governed by photochemical production and aerosol surface condensation loss, a steady state calculation is performed to evaluate GSA chemistry in Beijing. In general, simulated GSA captures the diurnal variations of measured GSA, indicating that condensation on preexisting aerosol surface corresponds to the dominant loss mechanism of GSA. Hence, GSA can potentially contribute to the aerosol aging process, considerably altering aerosol optical properties and hygroscopicity. GSA time series show a

ACPD
11, 5019–5042, 2011

wave shape pattern characterized by accumulation of aerosol followed by a washout. Analysis of the critical cluster composition using a multivariate statistical method indicates the presence of two sulfuric acid molecules. The calculated condensation rate of H_2SO_4 correlates with the daytime sulfate mass concentration of the Aitken mode, but not that of the accumulation mode aerosols. The results imply that condensation of GSA is likely responsible for the particle growth in the Aitken mode, but the growth in accumulation mode aerosols is more likely to be explained by inter-modal coagulation.

Acknowledgements. This work is part of the Campaign of Atmospheric Research in Beijing and surrounding areas supported by Beijing Environment Protection Bureau (OITC-G08026056) and the National Natural Science Foundation of China (20977001, 21025728). This work is also supported by the Robert A. Welch Foundation (Grant A-1417). R. Z. acknowledges further support from the National Natural Science Foundation of China Grant (40728006).

References

Arnold, F.: Atmospheric aerosol and cloud condensation nuclei formation: A possible influence of cosmic rays?, Space Sci. Rev., 125, 169–186, 2006.

Arnold, J. R., Hartsell, B. E., Luke, W. T., Ullah, S. M. R., Dasgupta, P. K., Huey, L. G., and Tate, P.: Field test of four methods for gas-phase ambient nitric acid, Atmos. Environ., 41, 4210–4226, doi:10.1016/j.atmosenv.2006.07.058, 2007.

Bohn, B., Corlett, G. K., Gillmann, M., Sanghavi, S., Stange, G., Tensing, E., Vrekoussis, M., Bloss, W. J., Clapp, L. J., Kortner, M., Dorn, H.-P., Monks, P. S., Platt, U., Plass-Dülmer, C., Mihalopoulos, N., Heard, D. E., Clemitshaw, K. C., Meixner, F. X., Prevot, A. S. H., and Schmitt, R.: Photolysis frequency measurement techniques: results of a comparison within the ACCENT project, Atmos. Chem. Phys., 8, 5373–5391, doi:10.5194/acp-8-5373-2008, 2008.

Chan, C. K. and Yao, X.: Air pollution in mega cities in China, Atmos. Environ., 42, 1–42, doi:10.1016/j.atmosenv.2007.09.003, 2008.

Cheng, Y. F., Wiedensohler, A., Eichler, H., Su, H., Gnauk, T., Brueggemann, E., Herrmann, H., Heintzenberg, J., Slanina, J., Tuch, T., Hu, M., and Zhang, Y. H.: Aerosol optical properties

ACPD

11, 5019–5042, 2011

and related chemical apportionment at Xinken in Pearl River Delta of China, Atmos. Environ., 42, 6351–6372, doi:10.1016/j.atmosenv.2008.02.034, 2008.
Cheng, Y. F., Berghof, M., Garland, R. M., Wiedensohler, A., Wehner, B., Muller, T., Su, H., Zhang, Y. H., Achtert, P., Nowak, A., Poschl, U., Zhu, T., Hu, M., and Zeng, L. M.: Influence of soot mixing state on aerosol light absorption and single scattering albedo during air mass aging at a polluted regional site in northeastern China, J. Geophys. Res., 114, D00G10, doi:10.1029/2008jd010883, 2009.
DeCarlo, P. F., Kimmel, J. R., Trimborn, A., Northway, M. J., Jayne, J. T., Aiken, A. C., Gonin, M., Fuhrer, K., Horvath, T., Docherty, K. S., Worsnop, D. R., and Jimenez, J. L.: Field-deployable, high-resolution, time-of-flight aerosol mass spectrometer, Anal. Chem., 78, 8281–8289, 2006.
Ehhalt, D. H. and Rohrer, F.: Dependence of the OH concentration on solar UV, J. Geophys. Res., 105, 3565–3571, 2000.
Fan, J. W. and Zhang, R. Y.: Atmospheric Oxidation Mechanism of Isoprene, Environ. Chem., 1, 140–149, doi:10.1071/en04045, 2004.
Finlayson-Pitts, B. J. and Pitts, J. N.: Chemistry of the upper and lower atmosphere : theory, experiments and applications, Academic Press, San Diego, Calif., xxii, 969 pp., 1999.
Ford, I. J.: Nucleation theorems, the statistical mechanics of molecular clusters, and a revision of classical nucleation theory, Phys. Rev. E, 56, 5615–5629, 1997.
Fortner, E. C., Zhao, J., and Zhang, R. Y.: Development of ion drift-chemical ionization mass spectrometry, Anal. Chem., 76, 5436–5440, doi:10.1021/Ac0493222, 2004.
Freiberg, J. E. and Schwartz, S. E.: Oxidation of SO_2 in aqueous droplets – mass-transport limitation in laboratory studies and the ambient atmosphere, Atmos. Environ., 15, 1145–1154, 1981.
Guo, S., Hu, M., Wang, Z. B., Slanina, J., and Zhao, Y. L.: Size-resolved aerosol water-soluble ionic compositions in the summer of Beijing: implication of regional secondary formation, Atmos. Chem. Phys., 10, 947–959, doi:10.5194/acp-10-947-2010, 2010.
He, S. Z., Chen, Z. M., Zhang, X., Zhao, Y., Huang, D. M., Zhao, J. N., Zhu, T., Hu, M., and Zeng, L. M.: Measurement of atmospheric hydrogen peroxide and organic peroxides in Beijing before and during the 2008 Olympic Games: chemical and physical factors influencing their concentrations, J. Geophys. Res., 115, D17307, doi:10.1029/2009JD013544, 2010.
Huang, X.-F., He, L.-Y., Hu, M., Canagaratna, M. R., Sun, Y., Zhang, Q., Zhu, T., Xue, L., Zeng, L.-W., Liu, X.-G., Zhang, Y.-H., Jayne, J. T., Ng, N. L., and Worsnop, D. R.: Highly time-

ACPD
11, 5019–5042, 2011

resolved chemical characterization of atmospheric submicron particles during 2008 Beijing Olympic Games using an Aerodyne High-Resolution Aerosol Mass Spectrometer, Atmos. Chem. Phys., 10, 8933–8945, doi:10.5194/acp-10-8933-2010, 2010.

IPCC: IPCC Fourth Assessment Report: Climate change 2007: the physical science basis, edited by: Solomon, S., Qin, D., Manning, M., Chen, Z., Marquis, M., Averyt, K. B., Tignor, M., and Miller, H. L., Cambridge Univ. Press, United Kingdom and New York, 996 pp., 2007.

Jefferson, A., Eisele, F. L., Ziemann, P. J., Weber, R. J., Marti, J. J., and McMurry, P. H.: Measurements of the H2SO4 mass accommodation coefficient onto polydisperse aerosol, J. Geophys. Res., 102, 19021–19028, 1997.

JPL: Chemical kinetics and photochemical data for use in atmospheric studies Evaluation 15, NASA, JPL, Caltech, Pasadena, Calif., 523 pp., 2006.

Khalizov, A. F., Xue, H. X., Wang, L., Zheng, J., and Zhang, R. Y.: Enhanced Light Absorption and Scattering by Carbon Soot Aerosol Internally Mixed with Sulfuric Acid, J. Phys. Chem. A, 113, 1066–1074, doi:10.1021/jp807531n, 2009a.

Khalizov, A. F., Zhang, R. Y., Zhang, D., Xue, H. X., Pagels, J., and McMurry, P. H.: Formation of highly hygroscopic soot aerosols upon internal mixing with sulfuric acid vapor, J. Geophys. Res., 114, D05208, doi:10.1029/2008jd010595, 2009b.

Kulmala, M., Vehkamaki, H., Petaja, T., Dal Maso, M., Lauri, A., Kerminen, V. M., Birmili, W., and McMurry, P. H.: Formation and growth rates of ultrafine atmospheric particles: a review of observations, J. Aerosol Sci, 35, 143–176, 2004.

Liu, Y. and Shao, M.: Estimation and prediction of black carbon emissions in Beijing City, Chin. Sci. Bull., 52, 1274–1281, doi:10.1007/s11434-007-0162-8, 2007.

McGraw, R. and Zhang, R. Y.: Multivariate analysis of homogeneous nucleation rate measurements. Nucleation in the p-toluic acid/sulfuric acid/water system, J. Chem. Phys., 128, 064508, doi:10.1063/1.2830030, 2008.

Metzger, A., Verheggen, B., Dommen, J., Duplissy, J., Prevot, A. S. H., Weingartner, E., Riipinen, I., Kulmala, M., Spracklen, D. V., Carslaw, K. S., and Baltensperger, U.: Evidence for the role of organics in aerosol particle formation under atmospheric conditions, P. Natl. Acad. Sci. USA, 107, 6646–6651, doi:10.1073/pnas.0911330107, 2010.

Molina, M. J., Molina, L. T., Zhang, R. Y., Meads, R. F., and Spencer, D. D.: The reaction of $ClONO_2$ with HCl on aluminum oxide, Geophys. Res. Lett., 24, 1619–1622, 1997.

Nadykto, A. B. and Yu, F. Q.: Strong hydrogen bonding between atmospheric nucleation precursors and common organics, Chem. Phys. Lett., 435, 14–18,

ACPD
11, 5019–5042, 2011

doi:10.1016/j.cplett.2006.12.050, 2007.
Seinfeld, J. H. and Pandis, S. N.: Atmospheric chemistry and physics: from air pollution to climate change, Wiley, New York, xxvii, 1326 pp., 1998.
Sipila, M., Berndt, T., Petaja, T., Brus, D., Vanhanen, J., Stratmann, F., Patokoski, J., Mauldin, R. L., Hyvarinen, A. P., Lihavainen, H., and Kulmala, M.: The Role of Sulfuric Acid in Atmospheric Nucleation, Science, 327, 1243–1246, doi:10.1126/science.1180315, 2010.
Suh, I., Lei, W. F., and Zhang, R. Y.: Experimental and theoretical studies of isoprene reaction with NO_3, J. Phys. Chem. A, 105, 6471–6478, 2001.
Wang, L., Khalizov, A. F., Zheng, J., Xu, W., Ma, Y., Lal, V., and Zhang, R.: Atmospheric nanoparticles formed from heterogeneous reactions of organics, Nature Geosci., 3, 238–242, http://www.nature.com/ngeo/journal/v3/n4/suppinfo/ngeo778_S1.html, 2010.
Wang, M., Zhu, T., Zheng, J., Zhang, R. Y., Zhang, S. Q., Xie, X. X., Han, Y. Q., and Li, Y.: Use of a mobile laboratory to evaluate changes in on-road air pollutants during the Beijing 2008 Summer Olympics, Atmos. Chem. Phys., 9, 8247–8263, doi:10.5194/acp-9-8247-2009, 2009.
Wang, T., Nie, W., Gao, J., Xue, L. K., Gao, X. M., Wang, X. F., Qiu, J., Poon, C. N., Meinardi, S., Blake, D., Wang, S. L., Ding, A. J., Chai, F. H., Zhang, Q. Z., and Wang, W. X.: Air quality during the 2008 Beijing Olympics: secondary pollutants and regional impact, Atmos. Chem. Phys., 10, 7603–7615, doi:10.5194/acp-10-7603-2010, 2010.
Young, L. H., Benson, D. R., Kameel, F. R., Pierce, J. R., Junninen, H., Kulmala, M., and Lee, S.-H.: Laboratory studies of H_2SO_4/H_2O binary homogeneous nucleation from the SO_2+OH reaction: evaluation of the experimental setup and preliminary results, Atmos. Chem. Phys., 8, 4997–5016, doi:10.5194/acp-8-4997-2008, 2008.
Yue, D. L., Hu, M., Zhang, R. Y., Wang, Z. B., Zheng, J., Wu, Z. J., Wiedensohler, A., He, L. Y., Huang, X. F., and Zhu, T.: The roles of sulfuric acid in new particle formation and growth in the mega-city of Beijing, Atmos. Chem. Phys., 10, 4953–4960, doi:10.5194/acp-10-4953-2010, 2010.
Zhang, D. and Zhang, R. Y.: Laboratory investigation of heterogeneous interaction of sulfuric acid with soot, Environ. Sci. Technol., 39, 5722–5728, 2005.
Zhang, D., Lei, W. F., and Zhang, R. Y.: Mechanism of OH formation from ozonolysis of isoprene: kinetics and product yields, Chem. Phys. Lett., 358, 171–179, 2002a.
Zhang, D., Zhang, R. Y., Park, J., and North, S. W.: Hydroxy peroxy nitrites and nitrates from OH initiated reactions of isoprene, J. Am. Chem. Soc., 124, 9600–9605, doi:10.1021/ja0255195,

ACPD
11, 5019–5042, 2011

2002b.
Zhang, Q. H., Zhang, J. P., and Xue, H. W.: The challenge of improving visibility in Beijing, Atmos. Chem. Phys., 10, 7821–7827, doi:10.5194/acp-10-7821-2010, 2010.
Zhang, R., Wooldridge, P. J., Abbatt, J. P. D., and Molina, M. J.: Physical-chemistry of the H_2SO_4/H_2O binary-system at low-temperatures – stratospheric implications, J. Phys. Chem., 97, 7351–7358, 1993.
Zhang, R. Y.: Getting to the Critical Nucleus of Aerosol Formation, Science, 328, 1366–1367, doi:10.1126/science.1189732, 2010.
Zhang, R. Y., Suh, I., Zhao, J., Zhang, D., Fortner, E. C., Tie, X. X., Molina, L. T., and Molina, M. J.: Atmospheric new particle formation enhanced by organic acids, Science, 304, 1487–1490, 2004.
Zhang, R. Y., Khalizov, A. F., Pagels, J., Zhang, D., Xue, H. X., and McMurry, P. H.: Variability in morphology, hygroscopicity, and optical properties of soot aerosols during atmospheric processing, P. Natl. Acad. Sci. USA, 105, 10291–10296, doi:10.1073/pnas.0804860105, 2008.
Zhang, R. Y., Wang, L., Khalizov, A. F., Zhao, J., Zheng, J., McGraw, R. L., and Molina, L. T.: Formation of nanoparticles of blue haze enhanced by anthropogenic pollution, P. Natl. Acad. Sci. USA, 106, 17650–17654, doi:10.1073/pnas.0910125106, 2009.
Zhao, J., Levitt, N. P., and Zhang, R. Y.: Heterogeneous chemistry of octanal and 2,4-hexadienal with sulfuric acid, Geophys. Res. Lett., 32, L09802, doi:10.1029/2004gl022200, 2005.
Zhao, J., Levitt, N. P., Zhang, R. Y., and Chen, J. M.: Heterogeneous reactions of methylglyoxal in acidic media: Implications for secondary organic aerosol formation, Environ. Sci. Technol., 40, 7682–7687, doi:10.1021/es060610k, 2006.
Zhao, J., Khalizov, A., Zhang, R. Y., and McGraw, R.: Hydrogen-Bonding Interaction in Molecular Complexes and Clusters of Aerosol Nucleation Precursors, J. Phys. Chem. A, 113, 680–689, doi:10.1021/jp806693r, 2009.
Zheng, J., Khalizov, A., Wang, L., and Zhang, R.: Atmospheric Pressure-Ion Drift Chemical Ionization Mass Spectrometry for Detection of Trace Gas Species, Anal. Chem., 82, 7302–7308, doi:10.1021/ac101253n, 2010.

ACPD
11, 5019–5042, 2011

Table 1. Summary of nucleation events during the CAREBeijing 2008 field study including aerosol formation rate (FR), GSA concentration, and relative humidity (RH%) that used in the multivariate analysis to evaluate the number of sulfuric acid molecule in the critical cluster.

Date	FR ($cm^{-3}\ s^{-1}$)	H_2SO_4 ($10^6\ cm^{-3}$)	RH %
12-Jul	7.3	5.0	27.8
17-Jul	13.2	7.1	40.8
1-Aug	6.9	4.8	58.9
12-Aug	13.2	7.4	63.4
15-Aug	8.7	5.5	51.5
18-Aug	2.1	3.2	50.5
23-Aug	7.3	6.3	41.2
31-Aug	5.8	4.5	47.3
1-Sep	4.2	5.3	40.8
18-Sep	2.4	4.0	44.3

ACPD
11, 5019–5042, 2011

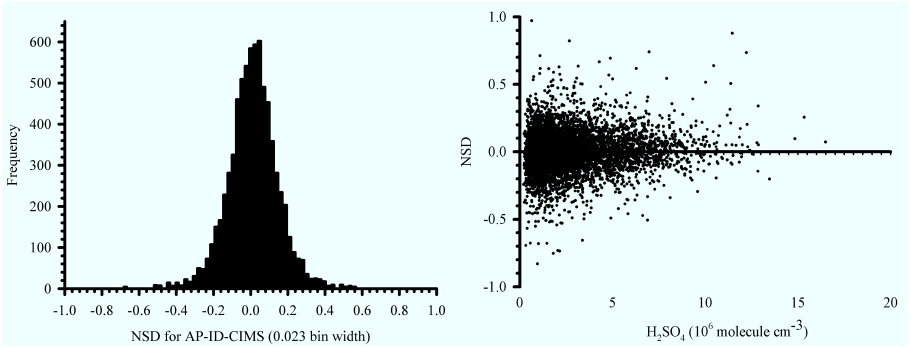

a b

Fig. 1. (a) Frequency histogram of normalized sequential difference (NSD) for the AP-ID-CIMS; **(b)** scatter plot of NSD with GSA concentration.

ACPD
11, 5019–5042, 2011

Measurements of gaseous H_2SO_4 by AP-ID-CIMS

J. Zheng et al.

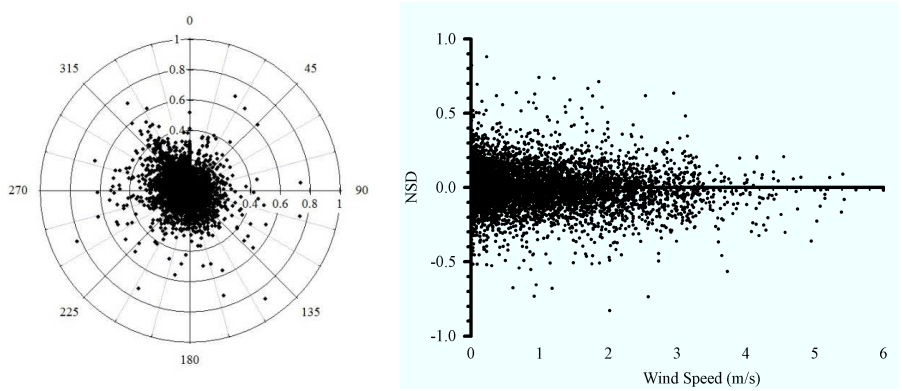

a b

Fig. 2. (a) A plot of NSD with wind direction (North represented by 0 degree). **(b)** A scatter plot of NSD with wind speed.

ACPD
11, 5019–5042, 2011

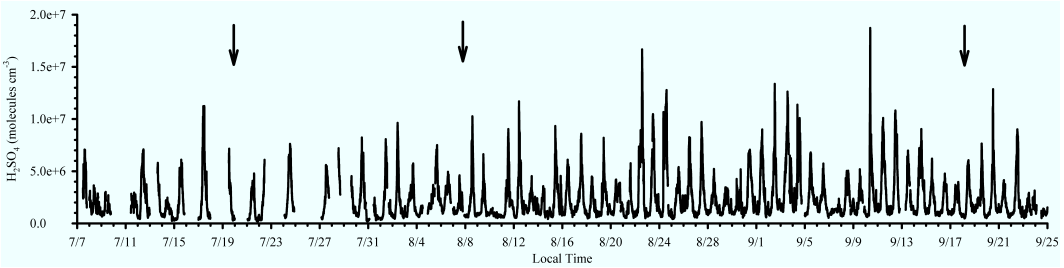

Fig. 3. Time series of 10 min averaged GSA concentration observed from 7 July to 25 September during the CAREBeijing 2008 Campaign. The arrows indicate the date of implementation of some major emission control measures, i.e., 20 July when odd/even plate number rule was applied, 8 August when full scale control was applied, and 18 September when the regulations were loosened.

ACPD
11, 5019–5042, 2011

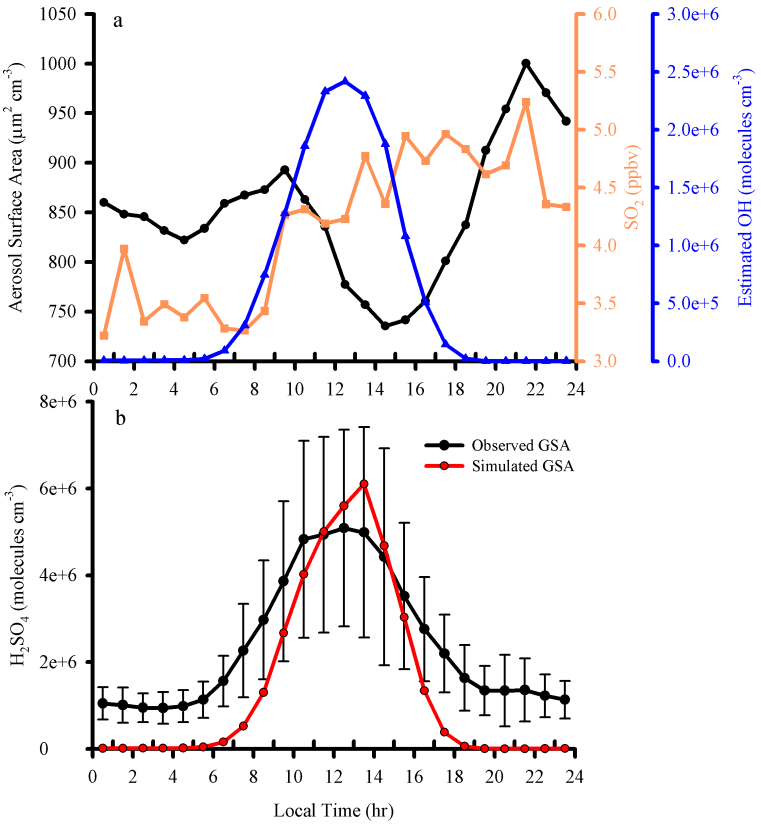

Fig. 4. (a) Hourly average diurnal profiles of aerosol surface area, SO_2, and modeled OH from 7 July to 25 September; **(b)** calculated (red) and measured (black) diurnal profiles of GSA.

ACPD
11, 5019–5042, 2011

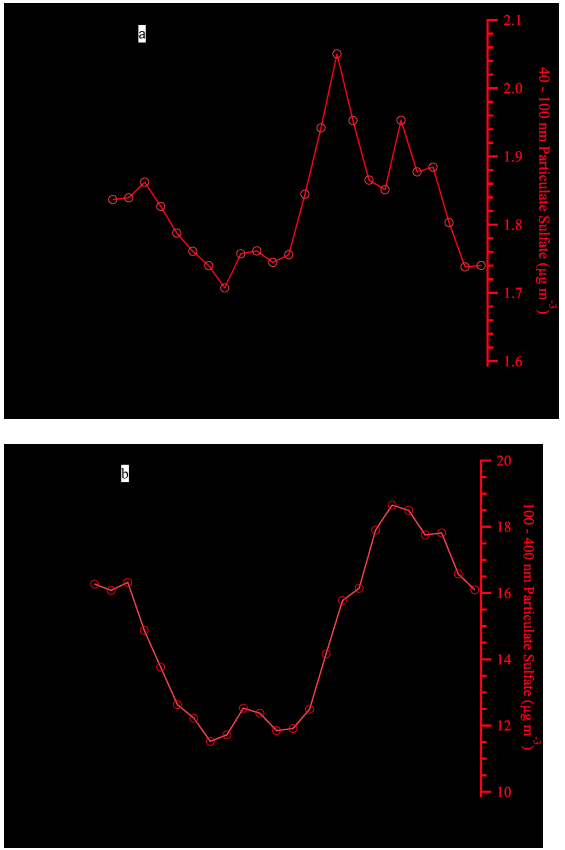

Fig. 5. **(a)** Diurnal profiles of condensation rates of GSA onto Aitken mode aerosols (40–100 nm) and sulfate concentrations in Aitken mode; **(b)** diurnal profiles of condensation rates of GSA onto accumulation mode particles (100–400 nm) and sulfate concentrations in accumulation mode.

ACPD
11, 5019–5042, 2011